Acta Crystallographica Section B
Structural Science
ISSN 0108-7681

Ab initio structure determination and Rietveld refinement of a high-temperature phase of zirconium hydrogen phosphate and a new polymorph of zirconium pyrophosphate from *in situ* temperature-resolved powder diffraction data

Anne Marie Krogh Andersen[a]* and Poul Norby[b]

[a]Department of Chemistry, University of Odense, DK-5230 Odense M, Denmark, and [b]Department of Chemistry, University of Oslo, N-0315 Oslo, Norway

Correspondence e-mail: amka@dou.dk

Received 15 November 1999
Accepted 15 February 2000

The collected *in situ* temperature-resolved synchrotron powder data revealed that the transformation of the recently reported three-dimensional τ-$Zr(HPO_4)_2$ to cubic ZrP_2O_7 goes through two intermediate phases. The first intermediate phase, ρ-$Zr(HPO_4)_2$, is formed in a reversible phase transition at 598 K, which involves both rearrangement and disordering of the hydrogen phosphate groups of τ-$Zr(HPO_4)_2$. At 688 K condensation of the hydrogen phosphate groups leads to the formation of the second intermediate, a new polymorph of zirconium pyrophosphate (β-ZrP_2O_7). Heating above 973 K results in the gradual transformation of β-ZrP_2O_7 to cubic zirconium pyrophosphate (α-ZrP_2O_7). The crystal structures of the two intermediate phases were solved from the *in situ* powder diffraction data using direct methods and refined using the Rietveld method. Both phases are orthorhombic, space group *Pnnm* and $Z = 2$. The lattice parameters for the two phases are: ρ-$Zr(HPO_4)_2$: $a = 8.1935\ (2)$, $b = 7.7090\ (2)$, $c = 5.4080\ (1)$ Å; β-ZrP_2O_7: $a = 8.3127\ (5)$, $b = 6.6389\ (4)$, $c = 5.3407\ (3)$ Å. The formation mechanism for the new zirconium pyrophosphate polymorph, β-ZrP_2O_7, is discussed in relation to structurally restricted soft chemistry.

1. Introduction

Layered phosphates with the general formula $M^{IV}(HPO_4)_2 \cdot nH_2O$ (M^{IV} = Zr, Ti *etc.*) have been studied extensively since the 1960s because of their ion exchange, intercalation and ion conduction properties (Clearfield, 1984; Alberti *et al.*, 1996). Recently we have synthesized and refined the structure of a unique new phase, τ-$Zr(HPO_4)_2$ (Krogh Andersen, Norby, Hanson & Vogt, 1998), with the same general formula as the layered phosphates. However, contrary to the previously known layered structures, this novel phase (unit-cell parameters $a = b = 11.259$, $c = 10.764$ Å; space group $I4_1cd$) has a three-dimensional framework structure. The structure is built from ZrO_6 octahedra which are linked together by HPO_4 tetrahedra, forming a framework with channels extending along the *c* axis. The hydroxyl groups of the HPO_4 groups point into the channels and form hydrogen-bonded spirals along the 4_1 axes. τ-$Zr(HPO_4)_2$ is, to our knowledge, the only framework structure among the $M^{IV}(HPO_4)_2 \cdot nH_2O$ materials. Thermogravimetric analysis of τ-$Zr(HPO_4)_2$ shows weight loss, indicating that condensation of the hydrogen phosphate groups occurs at 673 K (Krogh Andersen, Norby, Hanson & Vogt, 1998). The formation of layered pyrophosphates at low temperatures by the condensation of hydrogen phosphate

groups has previously been reported for α-$Zr(HPO_4)_2{\cdot}H_2O$ (Costantino & La Ginestra, 1982; Alberti & Costantino, 1984) and γ-$Ti(PO_4)(H_2PO_4){\cdot}2H_2O$ (Krogh Andersen & Norby, 1998).

In situ time- and temperature-resolved experiments is a powerful method of investigating chemical reactions such as the dehydration of zeolites (Ståhl *et al.*, 1996; Ståhl & Hanson, 1998), cation migration in zeolites (Norby *et al.*, 1998), phase transitions and thermal transformations (Christensen *et al.*, 1996; Krogh Andersen & Norby, 1998), intercalation reactions (Evans & O'Hare, 1994; Clark *et al.*, 1994) and hydrothermal synthesis of microporous materials (Cheetham & Mellot, 1997; Norby, 1997*b*; Christensen *et al.*, 1998; Norby & Hanson, 1998; Norby *et al.*, 1999). When taking advantage of high-intensity X-ray synchrotron radiation, combined with fast detectors (*e.g.* imaging plate, CCD or position-sensitive detectors) high-quality powder patterns suitable for full-profile Rietveld analysis can be recorded in minutes or even seconds (Norby, 1997*a*). This offers the possibility of following structural changes by Rietveld refinement in real time.

In this paper we report the results from investigations of the thermal transformations of τ-$Zr(HPO_4)_2$ using *in situ* temperature-resolved powder diffraction. Two hitherto unknown phases were discovered and characterized in the dehydroxylation and condensation process to cubic zirconium pyrophosphate (in the following denoted α-ZrP_2O_7).

2. Experimental

2.1. Synthesis of τ-$Zr(HPO_4)_2$

All reagents were of analytical grade and were used without further purification. τ-$Zr(HPO_4)_2$ was prepared by hydrothermal treatment of amorphous zirconium phosphate with 85% phosphoric acid, as described by Krogh Andersen, Norby, Hanson & Vogt (1998).

2.2. *In situ* data collection

In situ temperature-resolved synchrotron diffraction data were recorded at beamline X7B at the National Synchrotron Light Source (NSLS), Brookhaven National Laboratory (BNL). The data were collected with a Translating Image Plate (TIP) camera developed especially for time- and temperature-dependent experiments. An imaging plate was translated horizontally behind a steel screen with a 3 mm wide vertical slit. Heating of the sample was synchronized with the horizontal movement of the imaging plate, allowing a continuous series of powder diffraction patterns to be recorded on the imaging plate. The wavelength, sample-to-detector distance, imaging plate tilt and zero point were determined from a diffraction pattern of a LaB_6 standard sample (*NIST* SRM 660a, a = 4.15695 Å). The equipment as well as the data extraction and reduction are described in detail by Norby (1996, 1997*a*).

The samples were contained in open 0.5 mm quartz capillaries and heated with a heating rate of 15 K min^{-1} using an Enraf–Nonius heater gun. During data collection the samples were rotated to reduce the preferred orientation effects. The temperature was calibrated with a sample of microcrystalline silver metal, obtained by thermal decomposition of silver carbonate. The unit-cell parameter of silver was determined as a function of the measured temperature by profile refinement of the diffraction patterns collected during heating. The calibration curve was then determined by comparing the unit-cell parameters with literature values (Kuznetsov, 1956).

60 powder diffraction patterns were extracted from the imaging plate by integrating 30 pixels (3 mm) wide vertical rectangular strips (Norby, 1997*a*), corresponding to a temperature resolution of 15 K. In Fig. 1 the stack of powder patterns is shown as a function of temperature. For clarity only every second pattern is shown.

2.3. Collection of TG and DSC data

A thermogravimetric (TG) analysis was carried out with a SETARAM TG92-12 instrument. The heating rate was 5 K min^{-1} and the measurement was performed in nitrogen flow. Differential Scanning Calorimetry (DSC) was performed with a SETARAM DTA92-16.18 instrument with calcined Al_2O_3 as a reference. Heating and cooling rates of 5 and 10 K min^{-1} were used. The experiments were performed in an argon atmosphere.

2.4. NMR data collection

Solid-state ^{31}P MAS NMR spectra of α-ZrP_2O_7 and β-ZrP_2O_7 were obtained on a Varian XL-300 (7.1 T) spectrometer using a home-built MAS probe (Jakobsen *et al.*, 1988) and 7 mm o.d. (outside diameter) zirconia rotors (220 µl sample volume). The ^{31}P MAS NMR spectra were recorded using spinning speeds up to 7.0 kHz. Chemical shifts are given in p.p.m. relative to 85% H_3PO_4.

2.5. Structure determination and refinement

2.5.1. ρ-$Zr(HPO_4)_2$. A pattern of the pure phase was selected from the stack shown in Fig. 1 and indexed on the basis of the first 25 reflections using the auto-indexing

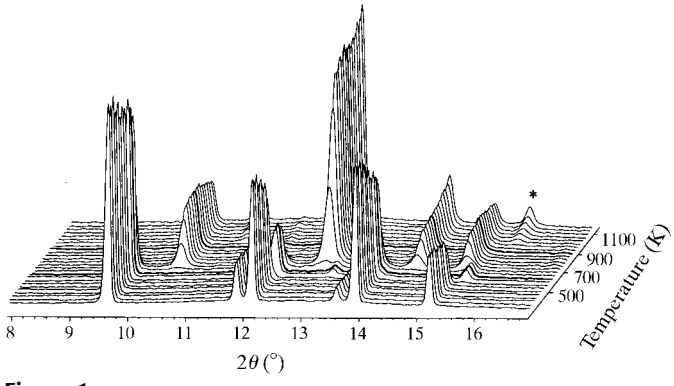

Figure 1
Three-dimensional representation of the *in situ* powder diffraction patterns as a function of temperature, showing the transformation of τ-$Zr(HPO_4)_2$ to cubic ZrP_2O_7. For clarity only every second pattern of the stack is shown. Patterns of pure ρ-$Zr(HPO_4)_2$ and β-ZrP_2O_7 are highlighted. * indicates α-ZrP_2O_7.

Table 1
Indexed powder pattern of ρ-$Zr(HPO_4)_2$ at 598 K.

Indexing based on an orthorhombic unit cell: a = 8.1856 (7), b = 7.6984 (7) and c = 5.4019 (5) Å.

hkl	d_{calc}	d_{obs}	Intensity	*hkl*	d_{calc}	d_{obs}	Intensity
110	5.6079	5.6077	100	341	1.5100	1.5105	7
101	4.5086	4.5060	31	422	1.5018	1.5022	6
011	4.4219	4.4231	36	051	1.4807	1.4807	3
200	4.0928	4.0897	13	033	1.4740	1.4739	4
111	3.8905	3.8884	62	242	1.4637	1.4635	5
210	3.6138	3.6144	22	133	1.4506	1.4506	4
120	3.4833	3.4827	13	323	1.4000	1.4009	4
211	3.0037	3.0017	44	251	1.3924	1.3924	4
121	2.9274	2.9271	39	512	1.3774	1.3776	6
220	2.8040	2.8034	26	004	1.3505	1.3507	5
002	2.7009	2.6997	19	350	1.3409	1.3406	3
310	2.5718	2.5704	7	413	1.3315	1.3315	4
221	2.4887	2.4879	5	152	1.3201	1.3205	4
112	2.4334	2.4327	13	114	1.3129	1.3132	4
031	2.3179	2.3179	9	611	1.3036	1.3031	4
202	2.2543	2.2520	4	143	1.2982	1.2979	3
320	2.2260	2.2265	4	060	1.2831	1.2844	3
022	2.2109	2.2104	6	423	1.2755	1.2755	3
212	2.1635	2.1628	4	214	1.2650	1.2655	3
122	2.1345	2.1343	4	161	1.2341	1.2339	3
321	2.0581	2.0581	6	224	1.2167	1.2166	5
231	2.0169	2.0163	9	451	1.1996	1.1997	3
222	1.9453	1.9453	18	433	1.1960	1.1962	4
330	1.8693	1.8681	16	343	1.1845	1.1841	3
312	1.8625	1.8607	13	631	1.1757	1.1755	2
132	1.8141	1.8136	10	622	1.1610	1.1610	3
141	1.7701	1.7703	8	710	1.1561	1.1560	3
240	1.7417	1.7413	5	253	1.1251	1.1252	3
113	1.7144	1.7152	6	550	1.1216	1.1219	2
232	1.6936	1.6931	4	640	1.1130	1.1133	2
241	1.6576	1.6566	3	334	1.0947	1.0949	4
402	1.6311	1.6308	6	552	1.0358	1.0357	3
213	1.6117	1.6115	8	125	1.0319	1.0319	3
430	1.5999	1.6002	9	225	1.0081	1.0080	3
042	1.5674	1.5673	7	732	0.9900	0.9899	2
511	1.5353	1.5356	11	471	0.9535	0.9534	3

program *TREOR*90 (Werner *et al.*, 1985). The program gave an orthorhombic solution with a figure of merit $M(20)$ = 30 (Wolff, 1968). The solution from *TREOR*90 was refined using the program *CELLKANT* (Ersson, 1981), giving the unit-cell parameters a = 8.1856 (7), b = 7.6984 (7) and c = 5.4019 (4) Å. The indexed powder pattern is presented in Table 1. The systematic absences [$h0l$ ($h + l = 2n + 1$) and $0kl$ ($k + l = 2n + 1$)] were consistent with space groups *Pnnm* (centrosymmetric) and *Pnn*2 (non-centrosymmetric). On the basis of the subsequent structure determination and refinement, the most likely space group was *Pnnm*. Integrated intensities were extracted in the range $8 < 2\theta < 50°$ using the Le Bail profile-fitting procedure (Le Bail *et al.*, 1988) with *GSAS* (Larson & Von Dreele, 1987). The extracted intensities were used as input for the direct-methods program *SIRPOW*92 (Altomare *et al.*, 1994; Cascarano *et al.*, 1992). An *E*-map computed for the solution with the best figure of merit revealed the position of the Zr, P and two O atoms. This structural model was used as a starting model for Rietveld refinement (Rietveld, 1969) using *GSAS*. After the initial refinement of the scale factor, background function, unit-cell parameters and profile parameters a difference Fourier map was calculated from which the positions of the remaining atoms were found. This procedure also revealed a disorder of the hydrogen phosphate group. Initially soft constraints were imposed on Zr—O and P—O bond distances. The weight of the constraints were gradually reduced and in the final stages of the refinement they were removed completely. All atoms were refined isotropically. Neutral atomic scattering factors, as stored in *GSAS*, were used for all atoms. No corrections were made for anomalous dispersion, preferred orientation or absorption. The final Rietveld refinement of the complete structure converged with $R(F^2)$ = 0.0706, R_{wp} = 0.0415, R_p = 0.0305 and χ^2 = 2.345. Experimental details, refined atomic coordinates and selected geometric parameters are given in Tables 2, 3 and 4, respectively. The final Rietveld difference plot is shown in Fig. 2.[1]

Table 2
Experimental details for data collection and Rietveld refinement.

	ρ-$Zr(HPO_4)_2$	β-ZrP_2O_7
Crystal data		
Chemical formula	$H_2O_8P_2Zr$	O_7P_2Zr
Chemical formula weight	283.18	265.16
Cell setting	Orthorhombic	Orthorhombic
Space group	*Pnnm*	*Pnnm*
a (Å)	8.1935 (2)	8.3127 (4)
b (Å)	7.7090 (2)	6.6389 (4)
c (Å)	5.4080 (1)	5.3407 (3)
V (Å^3)	341.59 (2)	294.74 (3)
Z	2	2
D_x (Mg m^{-3})	2.74	3.01
Radiation type	Synchrotron	Synchrotron
Wavelength (Å)	0.9336	0.9336
μ (mm^{-1})	1.04	1.20
Temperature (K)	598	778
Refinement		
$R(F^2)$	0.0706	0.0420
R_p	0.0305	0.0285
R_{wp}	0.0415	0.0367
$2\theta_{min}$ (°)	7.00	8.00
$2\theta_{max}$ (°)	49.84	44.86
χ^2	2.345	2.015
No. of reflections used in refinement	304	202
No. of parameters used	57	40
$(\Delta/\sigma)_{max}$	0.01	0.01

$R(F^2) = \Sigma|F_{hkl}(\text{obs})^2 - F_{hkl}(\text{calc})^2|/|F_{hkl}(\text{obs})^2|$; $R_{wp} = \{\Sigma w_i[y_i(\text{obs}) - y_i(\text{calc})]^2/\Sigma w_i[y_i(\text{obs})]^2\}^{1/2}$; $R_p = \Sigma|y_i(\text{obs}) - y_i(\text{calc})|/\Sigma y_i(\text{obs})$; $\chi^2 = \Sigma w_i[y_i(\text{obs}) - y_i(\text{calc})]^2/(N_{obs} - N_{var})$.

2.5.2. β-ZrP_2O_7. The unit-cell parameters for β-ZrP_2O_7 were determined as described above for ρ-$Zr(HPO_4)_2$. The solution from *TREOR*90 (Werner *et al.*, 1985), calculated from the first 22 reflections, had a figure of merit $M(20)$ = 25 (Wolff, 1968). The refined unit-cell parameters were a = 8.285 (2), b = 6.617 (2) and c = 5.325 (1) Å. The indexed powder pattern is provided in Table 5. The systematic absences were the same as for ρ-$Zr(HPO_4)_2$, giving the two possible space groups *Pnnm* and *Pnn*2. The subsequent Rietveld refinement showed that the most probable space group was *Pnnm* (see §3). The X-ray

[1] Supplementary data for this paper are available from the IUCr electronic archives (Reference: OS0045). Services for accessing these data are described at the back of the journal.

powder pattern was decomposed by the Le Bail method (Le Bail *et al.*, 1988) with the program *EXTRA* (Altomare *et al.*, 1995). The extracted intensities were used as input to *SIRPOW*92 (Altomare *et al.*, 1994; Cascarano *et al.*, 1992). An *E*-map calculated for the solution with the best figure of merit revealed the position of all the atoms in the structure. The structural model was used for Rietveld refinement (Rietveld, 1969) in *GSAS* (Larson & Von Dreele, 1987). The refinement was carried out as described for ρ-$Zr(HPO_4)_2$. However, it was not necessary to use soft constraints in the refinement. The final Rietveld refinement of the complete structure converged with $R(F^2) = 0.042$, $R_{wp} = 0.0367$, $R_p = 0.0285$ and $\chi^2 = 2.015$. Experimental details are given in Table 2. Selected geometric parameters and refined coordinates are given in Tables 4 and 6, respectively. The final Rietveld difference plot is shown in Fig. 3.

3. Results and discussion

3.1. Thermal behaviour

Thermogravimetric analysis of τ-$Zr(HPO_4)_2$ shows that one molecule of water per formula unit is lost at 673 K (Krogh Andersen, Norby, Hanson & Vogt, 1998). This loss corresponds to the condensation of two hydrogen phosphate groups to form a pyrophosphate group ($2HPO_4^{2-} \rightarrow P_2O_7^{4-} + H_2O$). The results of the differential scanning calorimetry (DSC) experiments show that there are two endotherms, at 598 and 688 K, before the transition to cubic zirconium pyrophosphate takes place at 1243 K. This indicates that two intermediate phases exist, which is in accordance with the transformations that can be observed from the *in situ* data shown in Fig. 1. The first transition was found to be reversible, as can clearly be seen from the DSC curve in Fig. 4. A small endotherm is seen just before the transition (at 588 K). However, no corresponding event can be seen in the diffraction experiments. The reversibility of the transition from τ-$Zr(HPO_4)_2$ to ρ-$Zr(HPO_4)_2$ can also be seen from the temperature-resolved *in situ* powder diffraction patterns (Fig. 5) with the temperature profile: 298 $\rightarrow$ 648 $\rightarrow$ 298 K. At approximately 973 K the formation of cubic zirconium pyrophosphate begins, indicated by the appearance of extra peaks at *e.g.* $2\theta = 16^\circ$ in Fig. 1.

The first transition takes place below the condensation temperature found from TG analysis, which indicates that the composition of the material is unchanged. Furthermore, it is found that the unit-cell volume of the first intermediate phase [ρ-$Zr(HPO_4)_2$] is close to a quarter of that of the starting compound τ-$Zr(HPO_4)_2$. This also corroborates the fact that no compositional change takes place in this transformation.

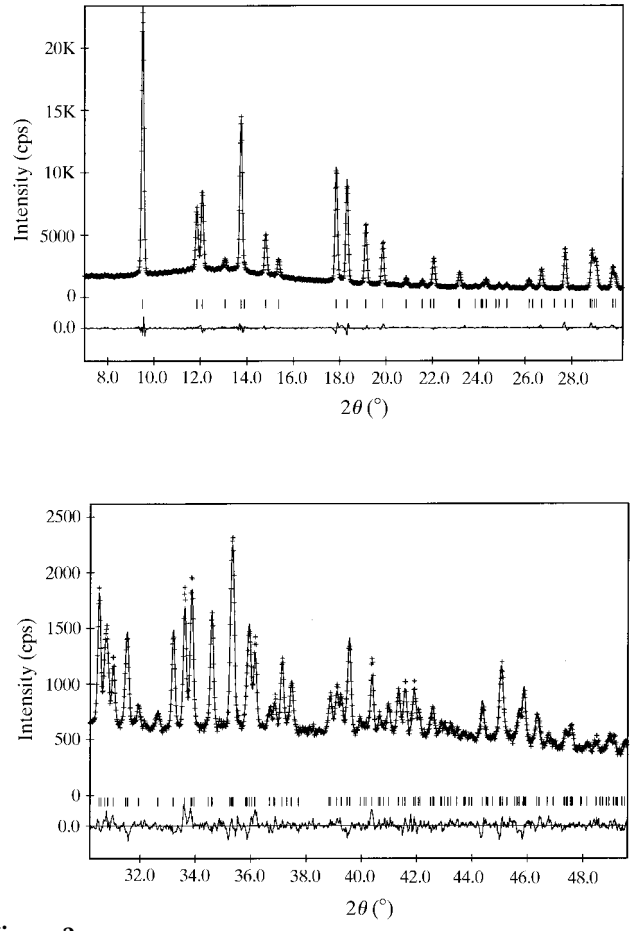

Figure 2
Observed (+), calculated (−) and difference profile for the final Rietveld refinement of ρ-$Zr(HPO_4)_2$.

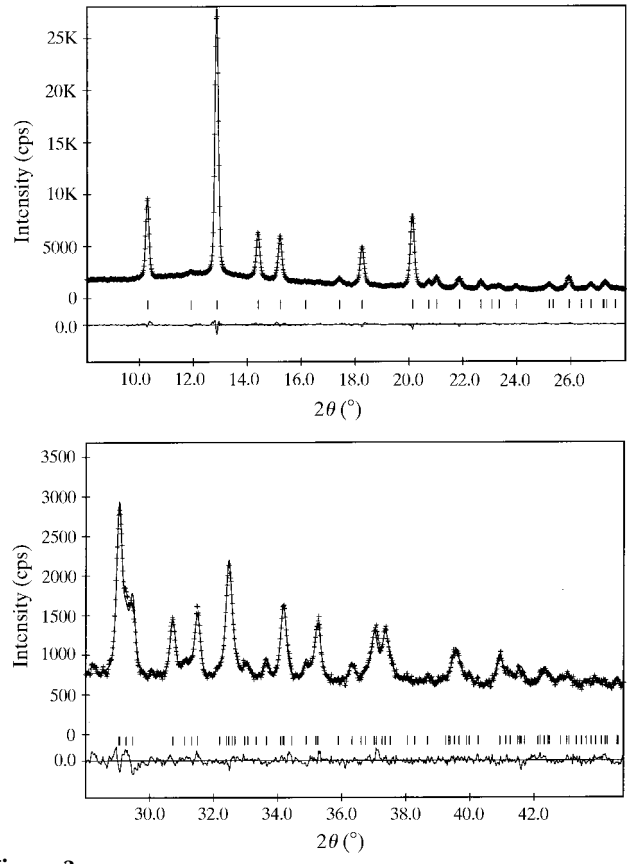

Figure 3
Observed (+), calculated (−) and difference profile for the final Rietveld refinement of β-ZrP_2O_7.

Table 3
Fractional atomic coordinates and equivalent isotropic displacement parameters (Å^2) for ρ-$Zr(HPO_4)_2$.

	Occupancy	x	y	z	U_{iso}
Zr	1	0	1/2	0	0.029 (1)
P1	1/2	0.3491 (10)	0.2442 (11)	0	0.040 (2)
P2	1/2	0.2776 (9)	0.1612 (9)	0	0.027 (2)
O1	1	0.3828 (6)	0.1475 (7)	0.7696 (7)	0.043 (2)
O2	1	0.1881 (9)	0.3234 (9)	0	0.032 (3)
O3	1/2	−0.0170 (3)	0.0990 (15)	1/2	0.100 (6)
O4	1/2	0.1479 (12)	0.016 (2)	0	0.040 (4)

Table 4
Selected geometric parameters (Å, °) for ρ-$Zr(HPO_4)_2$ and β-ZrP_2O_7.

	ρ-$Zr(HPO_4)_2$	β-ZrP_2O_7
Zr^{i}—$O1^{ii,\ iii,iv}$	2.084 (4) × 4	2.049 (6) × 4
Zr^{i}—$O2^{v,vi}$	2.056 (7) × 2	1.984 (11) × 2
P1—$O1^{vii}$	1.477 (6) × 2	1.471 (5) × 2
P1—O2	1.454 (11)	1.494 (9)
P1—$O3^{v}$	1.633 (16)	1.539 (4)
P2—$O1^{vii}$	1.519 (6) × 2	
P2—O2	1.450 (9)	
P2—O4	1.545 (14)	
O3—$O3^{viii}$	1.55 (2)	
$O3^{i}$—$O4^{v}$	3.090 (11)	
O4—$O4^{ix}$	2.44 (2)	
P1—P2	0.868 (9)	
$O1^{iv}$—Zr^{i}–$O1^{ii,iii}$	91.2 (2) × 2	90.1 (3) × 2
$O1^{ii}$—Zr^{i}—$O1^{iii,iv}$	180 × 2	180 × 2
$O1^{ii}$—Zr^{i}—$O1^{iii,iv}$	88.8 (2) × 2	89.9 (3) × 2
$O1^{ii,iii,iv}$—Zr^{i}—$O2^{v,vi}$	90.9 (2) × 4	89.2 (3) × 4
$O1^{ii,iii,iv}$—Zr^{i}—$O2^{v,vi}$	89.1 (2) × 4	90.7 (3) × 4
$O2^{v}$—Zr^{i}—$O2^{vi}$	180	180
$O1^{iv}$—P1—$O1^{vii}$	115.0 (7)	112.5 (6)
$O1^{vii}$—P1—O2	112.4 (5) × 2	113.6 (3) × 2
$O1^{vii}$—P1—$O3^{v}$	104.4 (6) × 2	105.2 (4) × 2
O2—P1—$O3^{v}$	107.4 (11)	105.9 (5)
$O1^{iv}$—P2—$O1^{vii}$	110.2 (6)	
$O1^{vii}$—P2—O2	110.3 (4) × 2	
$O1^{vii}$—P2—O4	109.9 (4) × 2	
O2—P2—O4	106.2 (9)	

† Symmetry codes: (i) $\frac{1}{2}+x, \frac{1}{2}-y, \frac{1}{2}+z$; (ii) $1-x, -y, -z$; (iii) $1-x, -y, 1-z$; (iv) $x, y, 1-z$; (v) $\frac{1}{2}+x, \frac{1}{2}-y, \frac{1}{2}-z$; (vi) $\frac{1}{2}-x, -\frac{1}{2}+y, \frac{1}{2}-z$; (vii) $x, y, z-1$; (viii) $1-x, 1-y, z$; (ix) $-x, -y, z$.

The temperature of the second transition corresponds to the condensation temperature determined from TG analysis. This indicates that the second intermediate (β-ZrP_2O_7) contains pyrophosphate groups.

3.2. ^{31}P MAS NMR results

The ^{31}P MAS NMR spectrum of α-ZrP_2O_7 shows 11 resonances in the range 35–44 p.p.m. This is in accordance with the existence of 11 phosphorus positions in the 3 × 3 × 3 superstructure of cubic zirconium pyrophosphate (Khosrovani *et al.*, 1996). The spectrum is very similar to the spectrum reported by Korthuis *et al.* (1995). An additional resonance at 45 p.p.m., which Korthuis *et al.* (1995) attributed to an impurity phase, is also present in our spectrum. However, we detected no impurity in the X-ray pattern of α-ZrP_2O_7. The ^{31}P NMR MAS spectrum of a quenched sample of β-ZrP_2O_7 shows only one single resonance at −39.6 p.p.m. The position corresponds well to the mean position found for α-ZrP_2O_7. This shows that there is only one phosphorus site in β-ZrP_2O_7. The resonance for β-ZrP_2O_7 is significantly broader than the individual resonances for α-ZrP_2O_7, which might be due to disorder of the bridging oxygen in the pyrophosphate group.

Table 5
Indexed pattern of β-ZrP_2O_7 at 778 K.

Indexing based on an orthorhombic unit cell: a = 8.285 (2), b = 6.617 (2) and c = 5.325 (1) Å.

hkl	d_{calc}	d_{obs}	Intensity
110	5.1703	5.1687	35
101	4.4797	4.4804	10
011	4.1486	4.1465	100
111	3.7096	3.7099	23
210	3.5112	3.5127	21
120	3.0725	3.0706	7
211	2.9314	2.9306	18
121	2.6613	2.6615	28
220	2.5852	2.5847	6
310	2.5486	2.5486	7
301	2.4516	2.4527	7
112	2.3672	2.3659	6
311	2.2989	2.3012	4
202	2.2399	2.2367	4
130	2.1314	2.1324	5
022	2.0743	2.0751	7
122	2.0122	2.0140	5
410	1.9767	1.9768	5
321	1.9698	1.9679	5
222	1.8548	1.8555	11
312	1.8411	1.8411	6
231	1.8285	1.8280	6
420	1.7556	1.7568	5
013	1.7145	1.7148	6
132	1.6640	1.6643	8
331	1.6397	1.6388	3
510	1.6074	1.6077	4
213	1.5842	1.5839	6
123	1.5370	1.5373	5
303	1.4932	1.4924	3
422	1.4657	1.4662	5
431	1.4526	1.4526	4
332	1.4468	1.4467	4
512	1.3761	1.3758	4
133	1.3640	1.3641	3
004	1.3313	1.3317	4
432	1.3134	1.3131	3

3.3. Structure of the intermediate phases

3.3.1. ρ-$Zr(HPO_4)_2$. The three-dimensional framework structure of ρ-$Zr(HPO_4)_2$ consists of corner-connected ZrO_6 octahedra and HPO_4 tetrahedra (Figs. 6*a* and *b*). The HPO_4 tetrahedra can be described by a disorder model with 50% population on each of two phosphorus (P1, P2) and two oxygen (O3, O4) sites. The O3—O3 ($-x, -y, z$) and O4—O4 ($-x, -y, z$) distances across the channel are 1.55 (2) and 2.44 (2) Å, respectively. The P1—P2 distance is 0.87 (1) Å. This imposes constraints on the population and local ordering

of the hydrogen phosphate groups. The structure is closely related to that of τ-$Zr(HPO_4)_2$. The half-diagonal in the tetragonal unit cell of τ-$Zr(HPO_4)_2$ becomes the orthorhombic a and b axes of ρ-$Zr(HPO_4)_2$ and the c axis is halved.

Refined coordinates and selected geometric parameters for ρ-$Zr(HPO_4)_2$ are given in Tables 3 and 4, respectively. The ZrO_6 octahedra are relatively regular, with bond lengths of 2.056 (7) and 2.084 (4) Å, and the largest deviation from the expected value of the O—Zr—O angle (90°) is 1.2°. These values compare well with previously reported Zr—O bonding angles and distances for zirconium hydrogen phosphates (Clearfield & Smith, 1969; Krogh Andersen, Norby, Hanson & Vogt, 1998). The two disordered phosphate tetrahedra show different distortions from regular tetrahedral geometry. In the $P1$ tetrahedron, where the condensation takes place, the P1—O3 bond of the P—OH group is 1.633 (16) Å, while the other three bonds average 1.469 (14) Å. This is in accordance with the observation that P—O bonds in P—OH groups generally are longer than P—O bonds in primary and secondary phosphates (Curry & Jones, 1971; Catti & Ivaldi, 1977; Krogh Andersen, Norby, Hanson & Vogt, 1998; Krogh Andersen, Norby & Vogt, 1998). The second of the disordered phosphate groups ($P2$) is more regular, with bond lengths varying from 1.450 (9) to 1.545 (14) Å, and angles from 106.2 (9) to 110.2 (6)°. As expected, the P2—O4 bond of the P—OH group is also significantly longer than the other P—O bonds in the tetrahedron. Thus, it is evident that the longer P—OH bonding distance of P1—O3 compared with P2—O4 result in a more distorted tetrahedron. The elongation of the P1—O3 bond in the $P1$ tetrahedron together with the orthorhombic distortion makes the O3—O3 $(-x, -y, z)$ distance short [1.55 (2) Å], facilitating the condensation reaction.

3.3.2. β-ZrP_2O_7. As seen in Figs. 7(*a*) and (*b*), the structure of β-ZrP_2O_7 is related to that of ρ-$Zr(HPO_4)_2$ (Figs. 6*a* and *b*). Comparing the unit-cell parameters of ρ-$Zr(HPO_4)_2$ and β-ZrP_2O_7 shows that the major difference is a shortening of the b axis from 7.7 to 6.6 Å, while the a and c axis are only slightly different. This is due to the condensation of the HPO_4 groups across the channel. The condensation involves only the hydroxyl groups of the $P1$ tetrahedra.

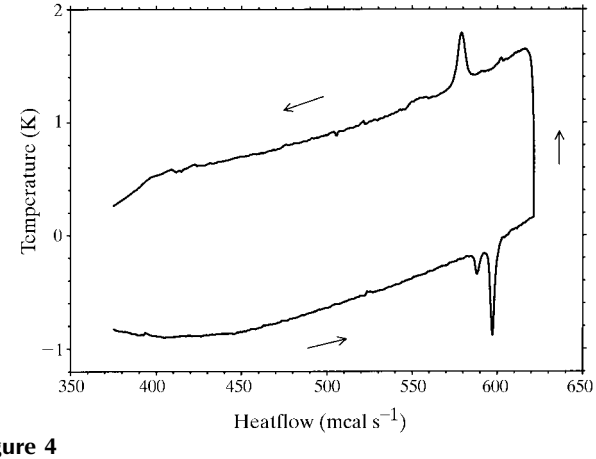

Figure 4
DSC for τ-$Zr(HPO_4)_2$ up to 648 K showing the reversibility of the first transition.

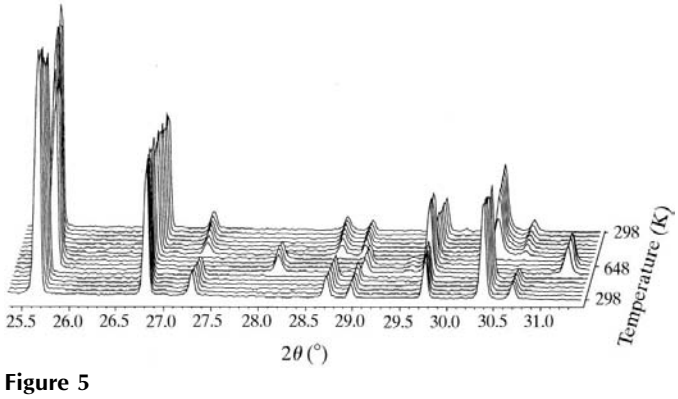

Figure 5
Three-dimensional representation of *in situ* powder diffraction patterns *versus* temperature (298 → 648 → 298 K), showing the reversibility of the first transition.

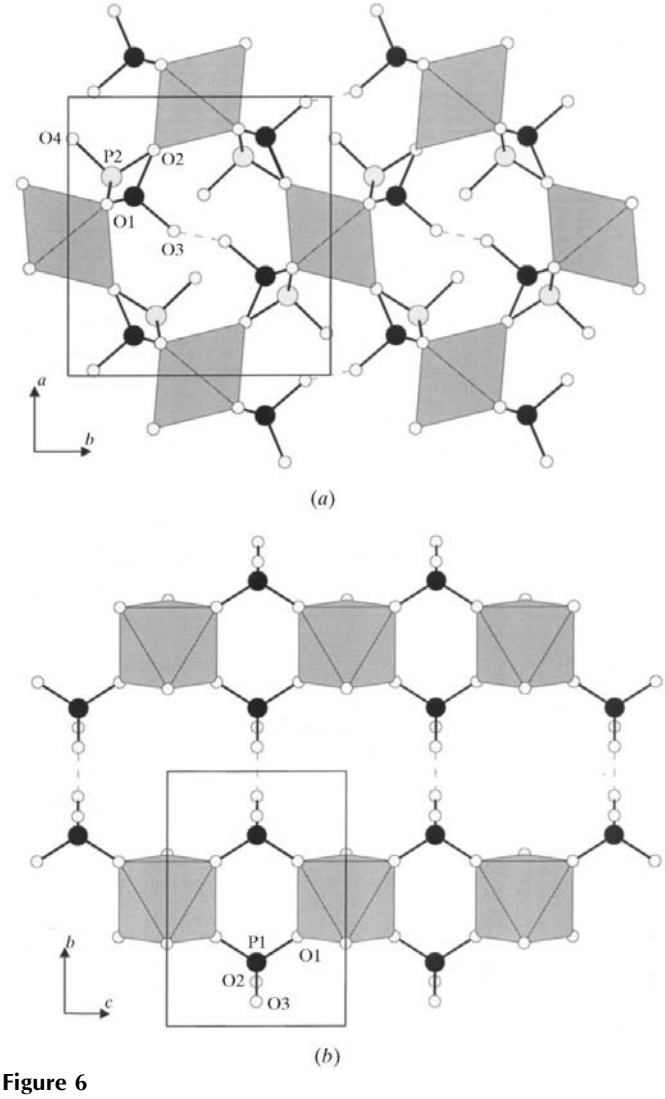

Figure 6
Structure of ρ-$Zr(HPO_4)_2$ seen along (*a*) [001] and (*b*) [100]. The dashed lines indicate where the condensation takes place. In Fig. 6(*b*) one of the disordered hydrogen phosphate groups has been omitted for clarity.

Selected geometric parameters and the final refined positions for β-ZrP_2O_7 are given in Tables 4 and 6, respectively. The ZrO_6 octahedra are regular, with an average Zr—O distance of 2.027 (20) Å and O—Zr—O angles in the range 89.2 (3)–90.7 (3)°. The PO_4 tetrahedra show regular geometry with average bond lengths [1.471 (5)–1.539 (4) Å] and angles [105.2 (4) to 113.6 (3)°]. The $P—O_T$ average distance (terminal oxygen) of 1.479 (11) Å is comparable to the average of the equivalent distances (1.514 Å) found in alkaline-earth and divalent transition metal pyrophosphates (Nord & Kierkegaard, 1980). The $P—O_B$ (bridging oxygen) distance [1.539 (4) Å] is also in good agreement with the distances found in these compounds, *i.e.* 1.55 Å. The bridging oxygen (O3) of the P_2O_7 group is situated on a center of symmetry and the P—O—P angle is therefore constrained to 180°. As can be seen in Table 6 this results in a fairly large thermal displacement parameter (U_{iso} = 0.10) for the bridging O3 atom, which might indicate a slight disorder of the O3 atomic position or possibly the wrong choice of space-group symmetry. A test was made to relax the symmetry constraints on the O3 position by Rietveld refinements in the other possible space group *Pnn*2. However, these refinements did not result in significantly reduced *R* values and the O3 position still displayed a large displacement parameter. Thus, the disorder model of the O3 position is favoured and the choice of space group is further corroborated.

Table 6
Fractional atomic coordinates and equivalent isotropic displacement parameters (Å^2) for β-ZrP_2O_7.

	x	*y*	*z*	U_{iso}
Zr	0	1/2	0	0.0370 (7)
P	0.3908 (6)	0.3129 (7)	0	0.047 (2)
O1	0.4335 (7)	0.2019 (9)	0.7710 (11)	0.058 (3)
O2	0.2222 (14)	0.3908 (12)	0	0.084 (4)
O3	0	0	1/2	0.107 (5)

β-ZrP_2O_7 is a new polymorph of zirconium pyrophosphate. It differs form the cubic polymorph (α-ZrP_2O_7) by having four and six rings of corner-connected polyhedra in the [100] direction and five rings in the [011] direction (see Fig. 8). The cubic polymorph, however, consists exclusively of five rings. Obviously the configuration of β-ZrP_2O_7 is energetically less favourable than that of its cubic counterpart. However, the transition directly to cubic zirconium pyrophosphate does not occur, because it is restricted by the structure of ρ-$Zr(HPO_4)_2$. This can be understood by looking at the condensation reaction ($2HPO_4^{2-} \rightarrow P_2O_7^{4-} + H_2O$). The condensation is a solid-state topotactic reaction, where the dehydroxylation is restricted by the crystal structure. In ρ-$Zr(HPO_4)_2$ the distance between OH groups at one of the two disordered hydrogen phosphate groups and the symmetry-related OH groups is 1.55 (2) Å [O3–O3 ($-x$, $-y$, z)]. These two oxygen positions in the hydrogen phosphate groups can therefore not be occupied simultaneously in a static way. However, this is where the condensation takes place, because the distance is favourable for dehydroxylation. The formation of β-ZrP_2O_7 is an example of a structurally restrained transformation, where a metastable polymorph is formed at low temperatures, *i.e.* a soft chemistry (*chimie douce*) process (Gopalakrishnan, 1995).

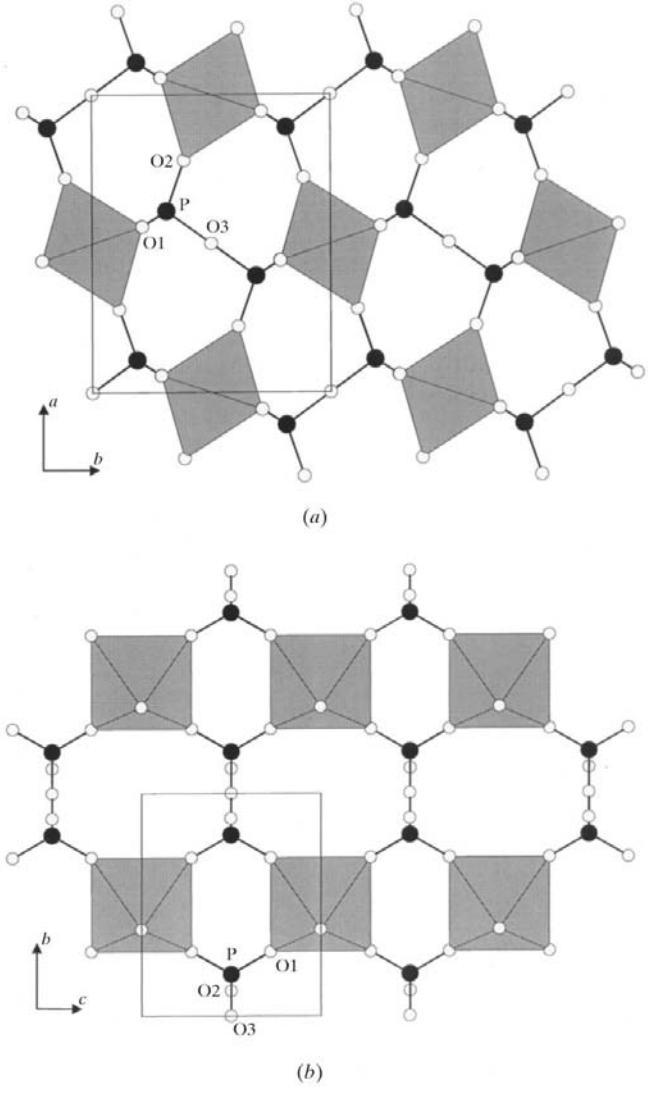

Figure 7
Structure of β-ZrP_2O_7 seen along (*a*) [001] and (*b*) [100].

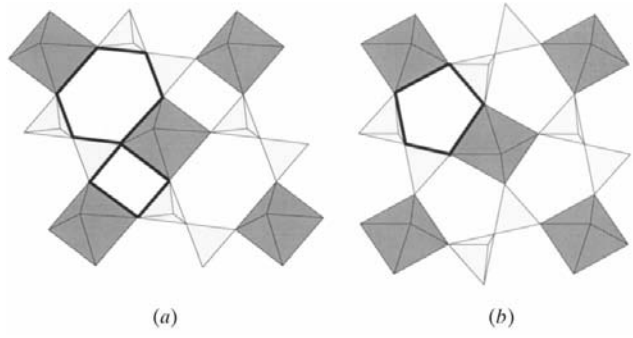

Figure 8
Schematic representation of the four, five and six rings of corner-connected polyhedra in β-ZrP_2O_7, highlighted with thick lines. Projection along (*a*) [100] and (*b*) [011].

4. Conclusions

The crystal structures of a new high-temperature phase of zirconium hydrogen phosphate, ρ-$Zr(HPO_4)_2$, and a new polymorph of zirconium pyrophosphate, β-ZrP_2O_7, have been solved and refined from *in situ* temperature-resolved powder diffraction data. The thermal transformations and dehydroxylation reactions of τ-$Zr(HPO_4)_2$ can be summarized as follows

$$\tau - Zr(HPO_4)_2 \overset{598\ K}{\longleftrightarrow} \rho - Zr(HPO_4)_2 \overset{688\ K}{\longrightarrow} \beta - ZrP_2O_7 \overset{1243\ K}{\longrightarrow} \alpha - ZrP_2O_7.$$

The transformation from ρ-$Zr(HPO_4)_2$ to β-ZrP_2O_7 can be viewed as a structurally restrained solid-state condensation.

We would like to thank J. C. Hanson in connection with the collection of synchrotron X-ray powder diffraction data and H. J. Jakobsen and H. Bildsøe for performing the MAS NMR measurements.

References

Alberti, G., Casciola, M., Costantino, U. & Vivani, R. (1996). *Adv. Mater.* **8**, 291–303.

Alberti, G. & Costantino, U. (1984). *J. Mol. Catal.* **27**, 235–250.

Altomare, A., Burla, M. C., Cascarano, G., Giacovazzo, C., Guagliardi, A., Moliterni, A. G. G. & Polidori, G. (1995). *J. Appl. Cryst.* **28**, 842–846.

Altomare, A., Cascarano, G., Giacovazzo, C., Guagliardi, A., Burla, M. C., Polidori, G. & Camalli, M. (1994). *J. Appl. Cryst.* **27**, 435–436.

Cascarano, G., Favia, C. & Giacovazzo, C. (1992). *J. Appl. Cryst.* **25**, 310–317.

Catti, M. & Ivaldi, G. (1977). *Z. Kristallogr.* **146**, 215–226.

Cheetham, A. K. & Mellot, C. F. (1997). *Chem. Mater.* **9**, 2269–2279.

Christensen, A. N., Norby, P. & Hanson, J. C. (1998). *Microporous Mesoporous Mater.* **20**, 349–354.

Christensen, A. N., Norby, P., Hanson, J. C. & Shimada, S. (1996). *J. Appl. Cryst.* **29**, 265–269.

Clark, S. M., Evans, J. S. O., O'Hare, D., Nuttall, C. J. & Wong, H.-V. (1994). *J. Chem. Soc. Chem. Commun.* pp. 809–810.

Clearfield, A. (1984). *Ann. Rev. Mater. Sci.* **14**, 205–229.

Clearfield, A. & Smith, G. D. (1969). *Inorg. Chem.* **8**, 431–436.

Costantino, U. & La Ginestra, A. (1982). *Thermochim. Acta*, **58**, 179–189.

Curry, N. A. & Jones, D. W. (1971). *J. Chem. Soc. A*, pp. 3725–3729.

Ersson, N. O. (1981). *CELLKANT.* Uppsala University, Sweden.

Evans, J. S. O. & O'Hare, D. (1994). *Adv. Mater.* **6**, 646–648.

Gopalakrishnan, J. (1995). *Chem. Mater.* **7**, 1265–1275.

Jakobsen, H. J., Daugaard, P. & Langer, V. J. (1988). *J. Magn. Reson.* **76**, 162–168; 19 April 1988, US Patent Number 4,739,270.

Khosrovani, N., Korthuis, V., Sleight, A. W. & Vogt, T. (1996). *Inorg. Chem.* **35**, 485–489.

Korthuis, V., Khosrovani, N., Sleight, A. W., Roberts, N., Dupree, R. & Warren, W. W. (1995). *Chem. Mater.* **7**, 412–417.

Krogh Andersen, A. M. & Norby, P. (1998). *Inorg. Chem.* **37**, 4313–4320.

Krogh Andersen, A. M., Norby, P., Hanson J. C. & Vogt, T. (1998). *Inorg. Chem.* **37**, 876–881.

Krogh Andersen, A. M., Norby, P. & Vogt, T. (1998). *J. Solid State Chem.* **140**, 266–271.

Kuznetsov, V. G. (1956). *Zh. Neorg. Khim.* **1**, 1548–1558.

Larson, A. & Von Dreele, R. B. (1987). Report No. LA-UR-86-748. Los Alamos National Laboratory, New Mexico, USA.

Le Bail, A., Duroy, H. & Fourquet, J. L. (1988). *Mater. Res. Bull.* **23**, 447–452.

Norby, P. (1996). *Mater. Sci. Forum*, **228–231**, 147–151.

Norby, P. (1997*a*). *J. Appl. Cryst.* **30**, 21–28.

Norby, P. (1997*b*). *J. Am. Chem. Soc.* **119**, 5215–5221.

Norby, P., Christensen, A. N. & Hanson, J. C. (1999). *Inorg. Chem.* **38**, 1216–1221.

Norby, P. & Hanson, J. C. (1998). *Catal. Today*, **39**, 301–309.

Norby, P., Poshni, F. I., Gualtieri, A. F., Hanson, J. C. & Grey, C. P. (1998). *J. Phys. Chem. B*, **102**, 839–856.

Nord, A. G. & Kierkegaard, P. (1980). *Chem. Scr.* **15**, 27–39.

Rietveld, H. M. (1969). *J. Appl. Cryst.* **2**, 65–71.

Ståhl, K., Artioli, G. & Hanson, J. C. (1996). *Phys. Chem. Miner.* **23**, 328–336.

Ståhl, K. & Hanson, J. C. (1998). *Eur. J. Mineral.* **10**, 221–228.

Werner, P. E., Eriksson, L. & Westdahl, M. (1985). *J. Appl. Cryst.* **18**, 367–370.

Wolff, P. M. (1968). *J. Appl. Cryst.* **1**, 108–113.